Negative Dielectric Constant of Water at a Metal Interface

Bolton Tran, Yuxing Zhou, Michael J. Janik, and Scott T. Milner*
Department of Chemical Engineering, The Pennsylvania State University, University Park, Pennsylvania 16802, USA

(Received 19 April 2023; accepted 9 November 2023; published 11 December 2023)

Water polarizability at a metal interface plays an essential role in electrochemistry. We devise a classical molecular dynamics approach with an efficient description of metal polarization and a novel ac field method to measure the local dielectric response of interfacial water. Water adlayers next to the metal surface exhibit higher-than-bulk in-plane and *negative* out-of-plane dielectric constants, the latter corresponding physically to overscreening of the applied field. If we account for the gap region at the interface, the average out-of-plane dielectric constant is quite low ($\epsilon_\perp \approx 2$), in agreement with reported measurements on confined thin films.

DOI: 10.1103/PhysRevLett.131.248001

Water at a metal interface plays a crucial role in aqueous electrochemical processes such as corrosion and electrocatalysis. Water molecules in the electrochemical double layer mediate electric field and solvation effects, which can significantly alter the energetics of elementary steps in electrochemical reactions [1–3]. The dielectric constant ϵ quantifies how well water molecules screen electric fields and solvate polar or charged species.

Recent experiments have inferred the dielectric constant of interfacial water from electrochemical capacitance measurements [4,5]; simulations can corroborate and rationalize experimental findings, by directly observing the local dielectric response of water molecules at the interface. Simulations of the water-metal interface have a long history [6–13]; but to our knowledge, simulations of the local dielectric polarizability of water at a metal interface are lacking.

Simulations of nanoconfined water between nonconducting surfaces have included studies of dielectric response for water in contact with model soft spheres [14], lipid bilayers [15], diamond surfaces [16], decanol surfaces [17,18], MXenes sheets [19], and graphene sheets [18,20–23]. These systems span a wide range of hydrophobic and hydrophilic surfaces, which are relevant to the behavior of water in biochemical processes, membrane ion transport, and nanocapacitors.

These simulation studies report markedly anisotropic dielectric response of water, with very different values for in-plane ($\epsilon_\parallel$) and out-of-plane ($\epsilon_\perp$) response. In-plane $\epsilon_\parallel$ values are often enhanced, while out-of-plane $\epsilon_\perp$ values are often suppressed compared to bulk water. Some simulation studies suggested a negative out-of-plane $\epsilon_\perp$ [16–19].

Experiments on the dielectric response of confined water likewise find conflicting results for the out-of-plane response. A recent experiment measured $\epsilon_\perp$ of about 2 for a 7 Å water layer confined between hexagonal boron nitride and graphite surfaces [4]. However, a negative dielectric constant was inferred by an experiment on water confined between MXenes nanosheets with salt [5]. These conflicting reports of abnormally low versus negative values of $\epsilon_\perp$ have not been reconciled.

In this Letter, we simulate the local in-plane and out-of-plane dielectric response of water at a single metal interface, with a sufficiently thick water layer to reach bulk behavior far from the metal; thus, we focus on interfacial effects, with no added complications from nanoconfinement. For the two water adlayers near the metal surface, we find that the local in-plane $\epsilon_\parallel$ is enhanced, and the local out-of-plane $\epsilon_\perp$ is negative. But when we combine the local negative values of $\epsilon_\perp$ with the contribution of the angstrom-scale gap at the interface, we find a low average value of $\epsilon_\perp \approx 2$ for interfacial water. This finding suggests a resolution of earlier conflicting results.

We use classical molecular dynamics (MD) to simulate water. Since the polarizability of liquid water is dominated by the response of H_2O dipoles (electronic polarizability contributes much less), classical MD is a suitable approach. Classical MD can access the length and timescales needed to sample the dynamic structure of interfacial water, whose dynamics are considerably slower than bulk water [13]. Our system consists of a one-layer-thick 30×17 Ag(111) orthogonal supercell (1020 Ag atoms), with 12096 SPC/E [24] water molecules. The cell z dimension is 9 nm, which includes a vapor space of about 4 nm above the water slab [Fig. 1(a)]. We used a 4 fs time step with the SETTLE constraint [25] on water molecules. Langevin dynamics [26] was used with a time constant of 2 ps to thermostat the system at 300 K. A pseudo-2D Ewalds scheme [27] was used for long-range electrostatics. Simulations were performed using GROMACS version 2016 [28]. Simulations ran at 45 ns/day with eight cores and one GPU. Data were collected for 100 ns for each

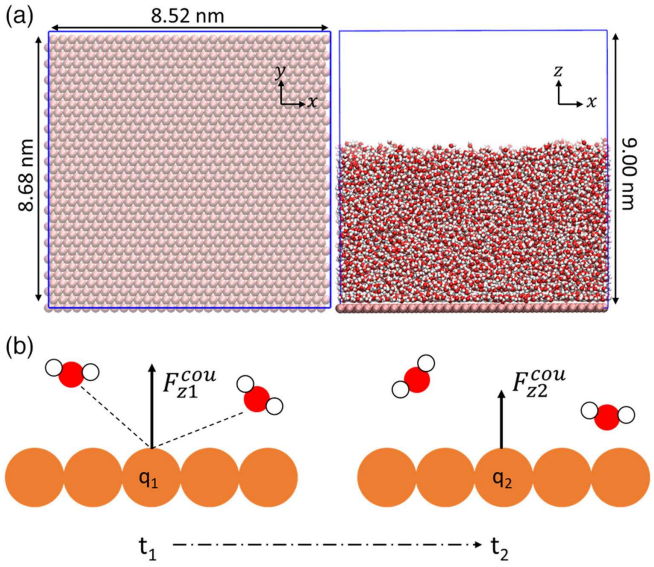

FIG. 1. (a) Snapshot of metal-water interface MD simulation with dimensions. (b) Illustration of the QDyn algorithm [see Eq. (1)].

in-plane and out-of-plane external field, following 1 ns of equilibration.

To give physically meaningful results, a simulation of the water-metal interface must account for polarization of the metal surface induced by nearby water molecules. A metal dynamically screens the electric field from the charge in the water layer by redistributing the metal surface charges. This surface charge distribution is equal in magnitude and opposite in sign, of a width set by the height of the charge above the surface.

Several approaches have been proposed to account for metal polarizability in classical MD [29]. These approaches include inserting fictitious image charges [8,30]; solving a discretized Poisson equation for surface charge density [31]; evolving a Drude model on each metal atom to represent mobile charges [32]; and using fluctuating Gaussian charge distributions at the surface [7]. These approaches require either computing additional terms in the periodic Coulomb potential or self-consistently solving coupled equations for surface charges with fictitious dynamics, which substantially increase the computational cost of the simulations. In this work, we introduce a new approach—named QDyn—that describes metal polarization with almost no additional computational cost.

QDyn discretizes the screening charge distribution for an ideal conducting plane onto a lattice of atoms. In the continuum limit, the surface charge distribution is explicitly given in terms of the incident field by Gauss' law. In QDyn, each metal atom bears a charge sufficient to cancel the normal field incident from the adjacent fluid. Because the simulation calculates Coulomb forces on all atoms, the normal field is known and the surface charges can be computed explicitly.

At each time step, the updated charge on each metal atom q_2 is computed from the charge q_1 and Coulomb force in the normal direction F_{z1}^{cou} in the previous time step [see Fig. 1(b)], according to

$$q_2 = 2\epsilon_o \frac{F_{z1}^{\mathrm{cou}}}{q_1} \frac{A}{N_q}, \tag{1}$$

where A is the metal surface area and N_q the number of metal atoms (for more details, see Supplemental Material [33]). Since F_{z1}^{cou} is already computed at every time step, the computational overhead is trivial: Store the charge q on each metal atom in an array, and update the charges using Eq. (1). QDyn is, therefore, much more efficient than previous metal polarization models [7,8,30–32].

For our simulation study, we chose silver due to its convenience in experimental studies: In open-circuit conditions, silver is rather inert, which avoids complications of chemisorbed water. Because QDyn treats all metals as ideal conductors, the chemical identity of the metal dictates only the lattice constant and the Lennard-Jones (LJ) parameters that describe short-range interactions between metal atoms and water. We fitted the LJ parameters between Ag-O and Ag-H to reproduce the water density profile and orientation distribution from an *ab initio* MD (AIMD) simulation [34], as shown in Fig. 2 (table of LJ parameters in Supplemental Material [33]).

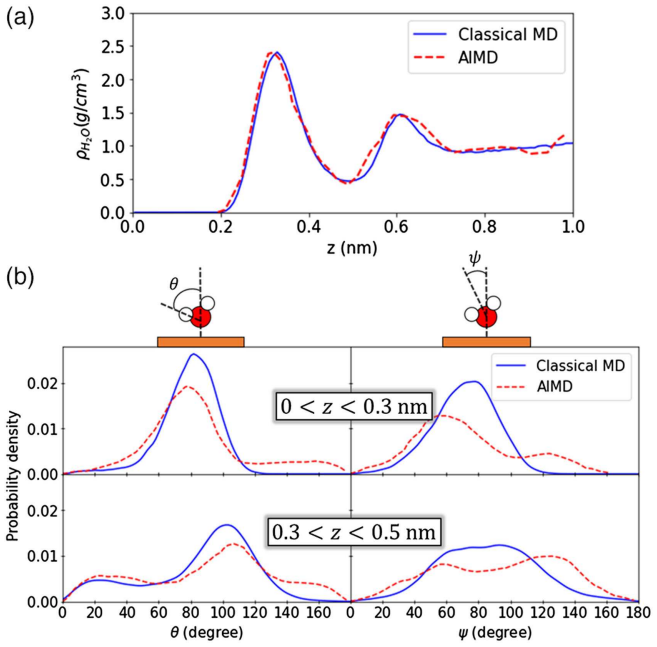

FIG. 2. (a) Water density profile using LJ parameters fitted to match the AIMD profile. (b) Probability distribution of angles between the HOH bisector or the OH bond and the z axis, in comparison with AIMD data. AIMD data were obtained from Le, Cuesta, and Cheng [34].

To improve the signal-to-noise ratio in simulating dielectric constants, we employ an alternating-current (ac) field response measurement. Previous works have measured dielectric response either by observing polarization fluctuation [17,21,22] or by measuring the polarization response to a static applied field [16,20,35]. Both approaches must contend with statistical error arising from thermal noise. By applying a slowly oscillating field to the system, the polarization response oscillates at the same frequency. The polarization time series can, thus, be filtered to remove almost all the Fourier components of the noise, for greatly improved signal-to-noise ratio (error analysis in Supplemental Material [33]). The statistics improve further, as the time series contains many periods of oscillation, so that the drive frequency is more precisely defined. We sample the ac response over 200 periods of oscillation; such long runs are possible thanks to the efficient QDyn algorithm.

Figure 3(a) illustrates the ac field procedure. The magnitude and frequency of the external field (red line) were chosen to stay within the linear response and quasistatic regimes of water polarizability. The polarization follows the oscillating applied field. Thermal noise is evident in the raw data (blue circles); Fourier filtering yields the polarization response (blue line). Further details of the method can be found in Supplemental Material [33].

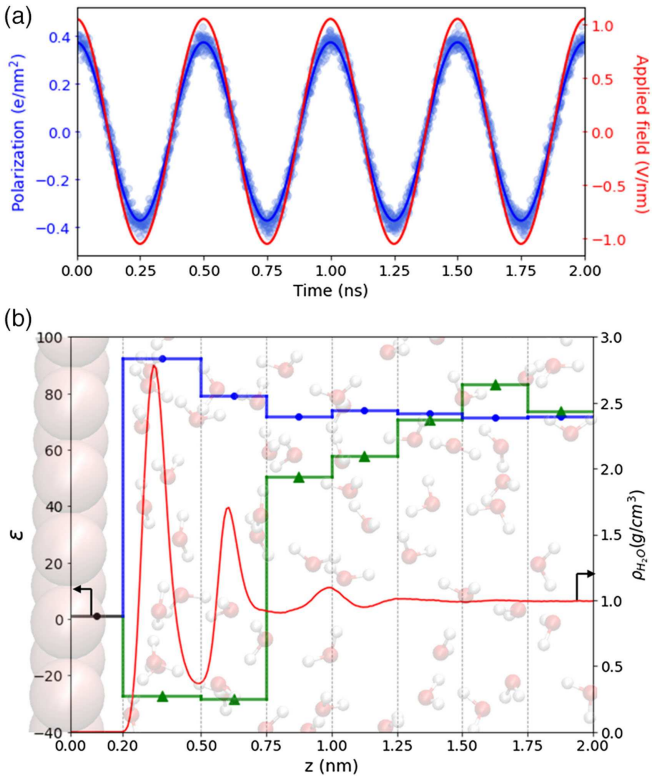

FIG. 3. (a) ac external electric field (red), polarization response raw data (blue circles), and Fourier-filtered response (blue line). (b) Out-of-plane $\epsilon_\perp$ (green triangle) and in-plane $\epsilon_\parallel$ (blue circle) dielectric constants in slabs at different distances from the surface. Statistical error bars of ϵ are too small to show. Water density (red) is overlaid.

We are interested in how the local dielectric constant varies with distance z from the metal surface. To measure the polarization in localized regions, we divide the z axis into bins; water molecules are assigned to a bin based on the location of their oxygen atoms.

We separately measure the in-plane and out-of-plane dielectric response, by applying fields parallel and normal to the surface in separate simulations. Because the in-plane polarization ($\parallel$) is homogeneous in the direction of the applied field, we determine the local dielectric constant with the usual permittivity equation [Eq. (2)]. But the out-of-plane polarization ($\perp$) is inhomogeneous in the z direction, so the dielectric response is computed taking into account the induced depolarization field [Eq. (3)]:

$$\epsilon_\parallel = 1 + \frac{P_\parallel}{\epsilon_o E_\parallel}, \tag{2}$$

$$\epsilon_\perp = 1 + \frac{P_\perp}{\epsilon_o E_\perp - P_\perp}. \tag{3}$$

The values of polarization $P_\perp$ or $P_\parallel$ and external field $E_\perp$ or $E_\parallel$ are taken from the amplitudes of their respective sinusoidal time series.

Figure 3(b) shows the resulting dielectric constant profiles. The choice of position and thickness of the virtual slices is guided by the water density profile (overlaid red line). Particularly interesting behaviors are observed for the first two "adlayers" of water (the first two peaks of the water density profile). Further from the surface (i.e., $z > 0.75$ nm), the in-plane and out-of-plane dielectric constants approach the bulk value (about 70 for SPC/E water).

Focusing on the near-surface behavior, the in-plane dielectric constants for the two adlayers are, respectively, about 30% and 13% larger than the bulk value. This enhanced in-plane polarizability had also been observed in simulations of nonmetal interfaces [14,17,22,36]. The out-of-plane dielectric constants of the two adlayers are negative. This behavior has been remarked upon in previous work on nonmetal interfaces [5,16,17,19]. Physically, negative dielectric constants correspond to overscreening of an external electric field. A normal dielectric screens and reduces an external field ($1 < \epsilon < \infty$). A perfect dielectric (i.e., a conductor) completely screens and cancels an external field ($\epsilon \to \infty$). An overscreening dielectric goes beyond perfect screening and produces a net field in the opposite direction of the external field ($-\infty < \epsilon < -1$).

Measuring the local dielectric constant by binning the molecules gives insight but has shortcomings. Spatial resolution is limited, and ambiguities arise in how we

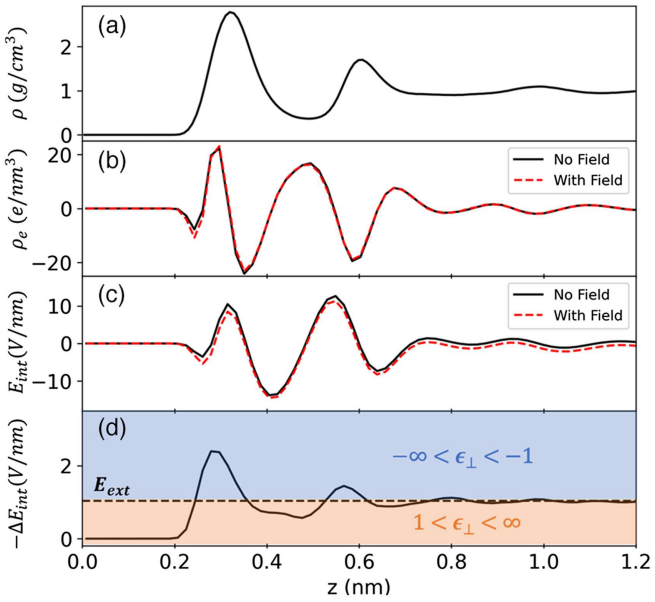

FIG. 4. (a) Mass density, (b) charge density, and (c) internal electric field with no external field (black solid line) and with external field (red dashed line). (d) Negative shift in the internal field (solid line) compared with the external field (dashed line).

define an occupied volume because water molecules protrude in and out of the bins, creating a rugged interface between bins. As an alternative, we bin water molecules into much finer slices and analyze the continuous profile of the internal electric field (Fig. 4).

The ordering of water near the metal surface [see Fig. 2(b)] gives rise to a nonzero charge density [Fig. 4(b)] and, consequently, a large internal electric field [Fig. 4(c)]. In response to an applied normal field, this charge density and internal field shifts as the molecules polarize (red dashed versus black solid lines). In this case, the applied field has a positive sign, and so the internal field shifts to the negative direction [the red dashed line is lower than the solid black line in Fig. 4(c)]. In Fig. 4(d), by comparing the shift of the internal field (ΔE_{int}) to the applied field (E_{ext}), we can interrogate the local dielectric response.

For a normal dielectric (i.e., $\epsilon > 1$), the shift in the internal field is of opposite sign and smaller than the external field ($-\Delta E_{\text{int}} < E_{\text{ext}}$). This corresponds to regular dielectric screening; the internal field shift reduces but does not completely cancel the applied field. This is the bottom region in Fig. 4(d). If the internal field shift becomes larger than the applied field ($-\Delta E_{\text{int}} > E_{\text{ext}}$), overscreening results. This is the negative dielectric constant regime ($-\infty < \epsilon < -1$) shown in the top region in Fig. 4(d).

Comparing the water mass density profile to the internal field shift [Figs. 4(a) and 4(d)], we observe a correspondence in the positions of peaks and troughs. In the two adlayers ($z = 0.3$ and $z = 0.6$ nm), water exhibits prominent overscreening behavior. This observation corresponds to the two negative values of $\epsilon_\perp$ in Fig. 3(b).

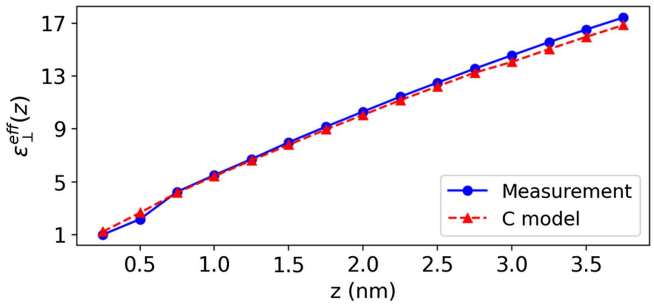

FIG. 5. Measured effective dielectric constant in comparison with the capacitor-in-series model. Here, z indicates the upper bound of a stack of multiple virtual slices.

Finally, we reconcile the observed negative values of $\epsilon_\perp$ [16,17,19] with the "abnormally low" values of $\epsilon_\perp$ [4,21] by applying a capacitor-in-series model [37] to account for the contribution of near-surface vacuum gaps to the average dielectric constant. The capacitor model assumes localized dielectric constants in a stack of slices and calculates an effective dielectric constant for the whole stack. Here, we cut the interface into slices of a thickness of $\Delta z = 0.25$ nm and measure the local dielectric constant of each slice. The effective out-of-plane dielectric constant for a stack of slices is

$$\epsilon_\perp^{\text{eff}}(z) = \frac{z}{\Delta z}\left(\sum_i^{z/\Delta z} \frac{1}{\epsilon_{\perp,i}}\right)^{-1}. \tag{4}$$

Here, $\epsilon_{\perp,i}$ denotes the local out-of-plane dielectric constant for slice i within the stack, and $\epsilon_\perp^{\text{eff}}(z)$ denotes the effective dielectric constant for the whole stack with upper bound z. Derivation of Eq. (4) can be found in Supplemental Material [33].

In Fig. 5, we show good agreement between the capacitor-in-series model from Eq. (4) and direct measurement of the effective dielectric constants for the entire region from the metal surface at $z = 0$ up to some z. The value of $\epsilon_\perp^{\text{eff}}(z < 0.25\ \text{nm})$ is about 1, which corresponds to the vacuum layer between the surface and the first water adlayer. We found $\epsilon_\perp^{\text{eff}}(z < 0.5\ \text{nm})$ to be about 2.5, which is the abnormally low value in excellent agreement with previous work [4,18,21,37].

The capacitor model resolves the conflict between negative near-surface values of $\epsilon_\perp$ in simulations and small positive values of $\epsilon_\perp$ in experiments. The local out-of-plane dielectric constant of the first water adlayer at $0.2\ \text{nm} < z < 0.5$ nm is negative [Fig. 3(b)], yet the effective value at $0.0\ \text{nm} < z < 0.5$ nm is 2.5 (Fig. 5). This low effective value stems from averaging in the permittivity of the vacuum region ($\epsilon_\perp = 1$).

In summary, we introduced a simulation model of the water-metal interface that accounts for metal polarizability as well as surface-induced structure and orientation. Using

an ac field approach, we observed unique dielectric behavior of water in the first two adlayers, namely, the higher-than-bulk in-plane and negative out-of-plane dielectric constants. We posit that the surface-induced order (Fig. 2), slow dynamics [8,13], and hydrogen bonding [22,36] among interfacial water molecules together give rise to such behavior. This resulting dielectric environment may substantially influence how ions can concentrate within the double layer, with consequences for electrochemical activation barriers and reaction rates.

The authors acknowledge funding from NSF-CBET 1939464 and support from the William H. Joyce Chair.

*stm9@psu.edu

[1] Q. Zhu, S. K. Wallentine, G.-H. Deng, J. A. Rebstock, and L. R. Baker, The solvation-induced Onsager reaction field rather than the double-layer field controls CO_2 reduction on gold, JACS Au **2**, 472 (2022).

[2] J. Gu, S. Liu, W. Ni, W. Ren, S. Haussener, and X. Hu, Modulating electric field distribution by alkali cations for CO_2 electroreduction in strongly acidic medium, Nat. Catal. **5**, 268 (2022).

[3] M. M. Waegele, C. M. Gunathunge, J. Li, and X. Li, How cations affect the electric double layer and the rates and selectivity of electrocatalytic processes, J. Chem. Phys. **151**, 160902 (2019).

[4] L. Fumagalli, A. Esfandiar, R. Fabregas, S. Hu, P. Ares, A. Janardanan, Q. Yang, B. Radha, T. Taniguchi, K. Watanabe, G. Gomila, K. S. Novoselov, and A. K. Geim, Anomalously low dielectric constant of confined water, Science **360**, 1339 (2018).

[5] A. Sugahara, Y. Ando, S. Kajiyama, K. Yazawa, K. Gotoh, M. Otani, M. Okubo, and A. Yamada, Negative dielectric constant of water confined in nanosheets, Nat. Commun. **10**, 850 (2019).

[6] K. Raghavan, K. Foster, K. Motakabbir, and M. Berkowitz, Structure and dynamics of water at the Pt(111) interface: Molecular dynamics study, J. Chem. Phys. **94**, 2110 (1991).

[7] J. I. Siepmann and M. Sprik, Influence of surface topology and electrostatic potential on water/electrode systems, J. Chem. Phys. **102**, 511 (1995).

[8] E. Spohr, Molecular simulation of the electrochemical double layer, Electrochim. Acta **44**, 1697 (1999).

[9] E. Spohr, Molecular dynamics simulations of water and ion dynamics in the electrochemical double layer, Solid State Ionics **150**, 1 (2002).

[10] A. P. Willard, S. K. Reed, P. A. Madden, and D. Chandler, Water at an electrochemical interface–a simulation study, Faraday Discuss. **141**, 423 (2009).

[11] D. T. Limmer, A. P. Willard, P. Madden, and D. Chandler, Hydration of metal surfaces can be dynamically heterogeneous and hydrophobic, Proc. Natl. Acad. Sci. U.S.A. **110**, 4200 (2013).

[12] D. T. Limmer, A. P. Willard, P. A. Madden, and D. Chandler, Water exchange at a hydrated platinum electrode is rare and collective, J. Phys. Chem. C **119**, 24016 (2015).

[13] D. T. Limmer and A. P. Willard, Nanoscale heterogeneity at the aqueous electrolyte-electrode interface, Chem. Phys. Lett. **620**, 144 (2015).

[14] V. Ballenegger and J. P. Hansen, Dielectric permittivity profiles of confined polar fluids, J. Chem. Phys. **122**, 114711 (2005).

[15] H. A. Stern and S. E. Feller, Calculation of the dielectric permittivity profile for a nonuniform system: Application to a lipid bilayer simulation, J. Chem. Phys. **118**, 3401 (2003).

[16] D. J. Bonthuis, S. Gekle, and R. R. Netz, Dielectric profile of interfacial water and its effect on double-layer capacitance, Phys. Rev. Lett. **107**, 166102 (2011).

[17] A. Schlaich, E. W. Knapp, and R. R. Netz, Water dielectric effects in planar confinement, Phys. Rev. Lett. **117**, 048001 (2016).

[18] P. Loche, C. Ayaz, A. Wolde-Kidan, A. Schlaich, and R. R. Netz, Universal and nonuniversal aspects of electrostatics in aqueous nanoconfinement, J. Phys. Chem. B **124**, 4365 (2020).

[19] H. Jalali, F. Khoeini, F. M. Peeters, and M. Neek-Amal, Hydration effects and negative dielectric constant of nano-confined water between cation intercalated MXenes, Nanoscale **13**, 922 (2021).

[20] E. J. Santos and E. Kaxiras, Electric-field dependence of the effective dielectric constant in graphene, Nano Lett. **13**, 898 (2013).

[21] H. Jalali, H. Ghorbanfekr, I. Hamid, M. Neek-Amal, R. Rashidi, and F. M. Peeters, Out-of-plane permittivity of confined water, Phys. Rev. E **102**, 022803 (2020).

[22] H. Jalali, E. Lotfi, R. Boya, and M. Neek-Amal, Abnormal dielectric constant of nanoconfined water between graphene layers in the presence of salt, J. Phys. Chem. B **125**, 1604 (2021).

[23] J. F. Olivieri, J. T. Hynes, and D. Laage, Confined water's dielectric constant reduction is due to the surrounding low dielectric media and not to interfacial molecular ordering, J. Phys. Chem. Lett. **12**, 4319 (2021).

[24] H. J. Berendsen, J. R. Grigera, and T. P. Straatsma, The missing term in effective pair potentials, J. Phys. Chem. **91**, 6269 (1987).

[25] S. Miyamoto and P. A. Kollman, Settle: An analytical version of the SHAKE and RATTLE algorithm for rigid water models, J. Comput. Chem. **13**, 952 (1992).

[26] N. Goga, A. J. Rzepiela, A. H. De Vries, S. J. Marrink, and H. J. Berendsen, Efficient algorithms for langevin and DPD dynamics, J. Chem. Theory Comput. **8**, 3637 (2012).

[27] I. C. Yeh and M. L. Berkowitz, Ewald summation for systems with slab geometry, J. Chem. Phys. **111**, 3155 (1999).

[28] M. J. Abraham, T. Murtola, R. Schulz, S. Páll, J. C. Smith, B. Hess, and E. Lindahl, GROMACS: High performance molecular simulations through multi-level parallelism from laptops to supercomputers, SoftwareX **1–2**, 19 (2015).

[29] L. Scalfi, M. Salanne, and B. Rotenberg, Molecular simulation of electrode-solution interfaces, Annu. Rev. Phys. Chem. **72**, 189 (2021).

[30] J. Hautman, J. W. Halley, and Y. J. Rhee, Molecular dynamics simulation of water between two ideal classical metal walls, J. Chem. Phys. **91**, 467 (1989).

[31] S. Tyagi, M. Süzen, M. Sega, M. Barbosa, S. S. Kantorovich, and C. Holm, An iterative, fast, linear-scaling method for computing induced charges on arbitrary dielectric boundaries, J. Chem. Phys. **132**, 154112 (2010).

[32] I. L. Geada, H. Ramezani-Dakhel, T. Jamil, M. Sulpizi, and H. Heinz, Insight into induced charges at metal surfaces and biointerfaces using a polarizable Lennard-Jones potential, Nat. Commun. **9**, 716 (2018).

[33] See Supplemental Material at http://link.aps.org/supplemental/10.1103/PhysRevLett.131.248001 for details about water-metal LJ potentials, the QDyn approach, the ac field method, and derivation of the capacitor-in-series model.

[34] J. Le, A. Cuesta, and J. Cheng, The structure of metal-water interface at the potential of zero charge from density functional theory-based molecular dynamics, J. Electroanal. Chem. **819**, 87 (2018).

[35] C. Zhang and M. Sprik, Computing the dielectric constant of liquid water at constant dielectric displacement, Phys. Rev. B **93**, 144201 (2016).

[36] H. Zhu, A. Ghoufi, A. Szymczyk, B. Balannec, and D. Morineau, Anomalous dielectric behavior of nanoconfined electrolytic solutions, Phys. Rev. Lett. **109**, 107801 (2012).

[37] C. Zhang, Note: On the dielectric constant of nanoconfined water, J. Chem. Phys. **148**, 156101 (2018).